BACHELOR

Dusty plasma parameter study and microwave resonance measurements

Zondag, Y.

Award date:
2014

Technische Universiteit
Eindhoven
University of Technology

Dusty plasma parameter study and microwave resonance measurements

Y. Zondag

22 juli 2014 EPG 14-08

Supervisor: F.M.J.H. Van de Wetering

Abstract

Dust particles are created in argon-acetylene radio-frequency plasmas. The formation of dust particles occurs in a matter of seconds to minutes after igniting the plasma. The plasma will fill with a cloud of particles up to micrometer sizes, the plasma is now a dusty plasma. After the dust cloud has been formed, dust-free zone develops in the plasma. This is called a void. The void suddenly stops growing and even shrinks, to shortly thereafter resume its expansion. This process is referred to as the hiccup. The hiccup is caused by coagulation of a new group of dust particles inside the void. This process is periodical and reproducible. The influence of the argon and acetylene gas flow on the shape of the void is investigated via laser light scattering. Furthermore, a measurement of the resonance spectrum of the cavity is done.

In this research an aluminium cavity is used with a metal mesh as the side wall. The dusty plasma and void are created inside the cavity. The void is not always an ellipsoid, when certain parameters are changed it can take a different form. It is also possible that there are random discharges at the bottom of the cavity which influence the void. The shape of the void is investigated by recording the laser light scattering on the dust particles. The different shapes of the void are given a certain color for each setting. When all measurement are completed it is investigated if the change in the gas flows is related to the shape of the void.

The MCRS (microwave cavity resonance spectroscopy) technique is used to determine the resonance spectrum of the cavity. By sending out microwaves by an antenna, standing electromagnetic field waves inside the cavity can occur. Some microwave frequencies excite standing waves at which the cavity serves as a resonator. Furthermore it is researched which resonant modes are excited during the measurement, both TM_{mnp} (transverse magnetic) and TE_{mnp} (transverse electric) modes.

Table of Contents

1 Introduction

1.1 Dusty plasma

A dusty plasma is, as the name suggests, a plasma with dust particles inside. These particles are highly charged and significantly alter the properties of the plasma. Dusty plasma can be used to study various physical phenomena like lattice waves, melting and annealing, because the dust particles can be visualized more easily than individual atoms. Some examples of dusty plasmas in space are interplanetary dust, tails of comets and the Earth's (upper) atmosphere [4].

1.2 Goals

One of the goals in this research was to investigate the influence of the argon and acetylene gas flow on the void in a dusty plasma. To determine the shape of the void a laser and camera are used. The laser light will scatter on the dust particles inside the plasma. A laser line filter ensures that only the scattered light will reach the camera. The different shapes of the void are given a certain color for each setting.
The second goal is to the measure the resonance spectrum of the cavity and to determine which resonance modes are excited in the cavity. The spectrum is measured with the help of two antennas inside the cavity. One antenna emits microwaves, the other one serves as a detector. When a signal is sent through the cavity, transverse magnetic (TM) and transverse electric (TE) modes can occur in the cavity. The frequencies of certain modes are calculated for an ideal cavity and plotted with the spectrum. When the spectrum has a peak at one of the modes, it is possible that this mode did occur in the cavity.

2 Theory

2.1 Plasma

A plasma is formed when gas is ionized. Heating a gas may ionize its molecules or atoms (creating charged particles such as ions and electrons), thus turning it into a plasma. Ionization can be achieved in a few different ways, for example by a strong electromagnetic field generated by, for example, a laser or a radio-frequency (RF) signal. In this research a plasma is created by applying a high RF voltage to the upper plate of a small cylindrical metal box called the cavity.
A plasma has similar conductive properties as metals. It is the most occurring form of matter in the Universe; interstellar clouds, stellar coronas and stars like the sun are all in plasma phase [4].
Figure 2.1 shows the plasma created between two flat electrodes. A plasma can be divided into two parts: a bulk and a sheath. The plasma does not exists near the two plates of the cavity. These areas are the sheaths. In the middle of the cavity the plasma is formed, this is the bulk.

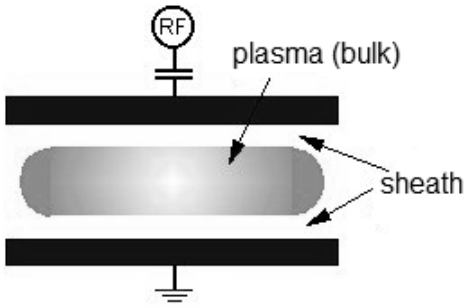

Figure 2.1: *Plasma between to flat electrodes with bulk and sheath indicated.*

2.2 Dusty plasma

A dusty plasma is a plasma which contains nanometer (10^{-9} m) to micrometer (10^{-6} m) sized particles. These particles are charged by the plasma (due to high electron mobility) and, as a benefit or nuisance depending on the application, influence the plasma. A plasma is quite complex because of all the ions and electron it contains, but a dusty plasma is even more complex. Due to this additional complexity of studying plasmas with charged dust particles, dusty plasmas are also known as complex plasmas and for its resemblance with complex fluids [2, 3].

2.2.1 Dust particles

Almost any (inert) gas can be used to create a plasma, but to make a dusty plasma a reactive gas has to be added to the gas flow. When the plasma is ignited, small dust particles will start to fill the plasma, almost in all cases initiated by polymerization of monomers formed from the reactive gas. These dust particles will levitate inside the cavity due to several forces (section 2.3). Under certain conditions [8–10], the particles form a dust cloud and after a while a dust-free zone develops. Usually this zone has the shape of an ellipsoid and is called a dust void [1].

2.2.2 Growth of the particles

For silane (SiH_4) the growth of the dust particles takes place in four stages [3] (shown in figure 2.2), but is believed to hold also for the reactive gas used in this research: acetylene (C_2H_2).

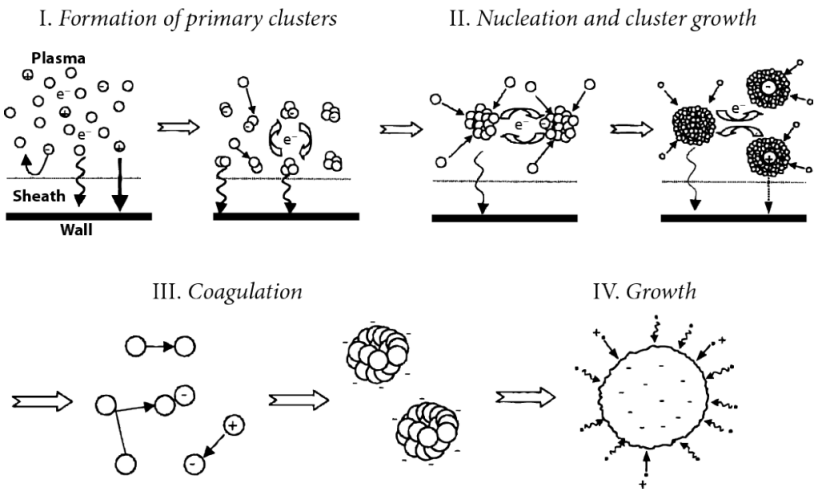

Figure 2.2: *The growth of the dust particles.*

1. Formation of primary clusters.
When the acetylene is injected in the plasma, the acetylene molecules can polymerize due to the free electrons inside the plasma. These electrons are created by electron-impact ionization of argon:

$$\mathrm{Ar} + \mathrm{e}^- \rightarrow \mathrm{Ar}^+ + 2\mathrm{e}^-. \tag{2.1}$$

The electrons react with the the acetylene gas

$$\mathrm{C_2H_2} + \mathrm{e}^- \rightarrow \mathrm{C_2H}^- + \mathrm{H}. \tag{2.2}$$

The polymerization reaction is given by [2, 4]:

$$\mathrm{C_2H}^- + \mathrm{C_2H_2} \rightarrow \mathrm{C_4H}^- + \mathrm{H_2}. \tag{2.3}$$

Or in generalized form:

$$\mathrm{C_{2}{}_{n}H}^- + \mathrm{C_2H_2} \rightarrow \mathrm{C_{2}{}_{n+2}H}^- + \mathrm{H_2}, \tag{2.4}$$

with n a positive integer.
Especially the negative ions contribute to the dust formation process, because the positive ions are attracted by the wall of the cavity and the neutral particles leave the plasma through diffusion.

2. Nucleation.
The polymerized clusters from stage 1 can stick together. This happens when the dust particles have reached a certain (critical) radius (of about 2 to 5 nm), the particles will transit from the gas phase to the solid state. This is called nucleation.

3. Coagulation.
Before this stage, the clusters are mainly neutral or single charged. Coagulation occurs for many particles at the same time when they reach a critical density. After the coagulation the dust particles are large enough to act as tiny plasma probes. Therefore they attract a lot of electrons, which means that the electron density inside the plasma will drop. The dust particles are a sink for electrons.

4. Growth.
The dust particles continue to grow in size due to adsorption of plasma species such as ions and radicals. When the particles reach a certain size, they will leave the cavity due to the gravity pull (if the experiment is carried out on Earth). This will cause a decrease in the strength of the sink of free electrons. During the plasma's response to this new situation, the electron density will increase, until ionization is at an equilibrium again.

2.3 Forces acting on dust particles

In the plasma, various forces act on the dust particles. The forces scale differently with particle size. This means that the location of the particle determines if the particle is trapped in the plasma. The following forces will be briefly discussed [4–6]:

1. Gravity
A dust particle is subject to gravity with a force that is proportional to its mass m. This force can be written as

$$F_g = mg = \frac{4}{3}\pi a^3 \rho g, \tag{2.5}$$

where g is the local acceleration, ρ the mass density of the particle and a is the radius of a particle. For sub micron particles, this force can be neglected, but not for larger particles. Gravity can be the dominant force which limits the time the particle stays in the plasma.

2. Electric force
The electric force acting on dust particles of charge Q is equal to

$$F_e = QE. \tag{2.6}$$

The electric field E is larger in sheaths near the plasma wall boundary and smaller in the bulk.

3. Neutral drag force
This force is the result of the collisions of the particles with neutral gas atoms or molecules. The force is proportional to the neutral gas pressure in the setup.

$$F_n = \frac{4}{3}\pi r_p^2 m_N n_N v_{th,N}(u_N - u_p), \tag{2.7}$$

where r_p is the radius of the dust particle, m_N the mass of the neutral atoms, n_N the neutral (number) density, $v_{th,N}$ the thermal velocity of the neutrals, u_N the neutral gas particles speed and u_p the dust particles speed. Note that u_N - u_p is the relative speed of the dust particles with respect to the gas flow speed.

4. Ion drag force
The ion drag force is due to the transfer of momentum to dust particles by collisions with ions. Especially at the boundaries of the plasma, where positive ions are accelerated in the sheath electric field, the total momentum of the positive ions might become significant, but the force already plays an important role in the formation of the dust void.

5. Thermophoretic force
A third drag force, the thermophoretic force F_{th}, based on momentum transfer as well, is due to a temperature gradient in the gas. The neutral gas atoms or molecules on the hot side of the dust particles have a higher thermal velocity and will transfer more momentum to the particle than those on the cold side when a collision occurs. This results in a net momentum transfer and thus in a force on the particle in the same direction as the temperature gradient.

6. Radiation pressure force
The radiation pressure force is initiated when dust particles are irradiated with directed electromagnetic radiation, such as a strong laser. The fraction of radiation energy intercepted by the dust particle results into a net momentum transfer and consequently into a net force working on the particle. This force is usually not significant when no or weak (illumination) lasers are used.

2.4 Resonance

Not only the void is investigated in this research, but also the electro-magnetic resonance of the cavity for microwaves. Two antennas are placed inside the cavity. One antenna emits microwaves, the other one serves as a detector. When microwaves are introduced into a cylindrical cavity, two types of standing waves can occur in the closed cavity: transverse magnetic (TM) and transverse electric (TE) modes. TM modes do not have a magnetic field in the direction of the propagation, whereas TE modes have no electric field in the direction of propagation [7]. In ideal circumstances, i.e. a perfect cavity, the field patterns can be calculated. The equations used to calculate the modes are as follows (in cylindrical coordinates):

$$k_3 = \frac{p\pi}{d}, \tag{2.8}$$

$$k^2 = k_1^2 + k_3^2, \tag{2.9}$$

$$E = \sqrt{E_r^2 + E_\phi^2 + E_z^2}. \tag{2.10}$$

For the TM modes, the following equations are used:

$$k_1 = \frac{x_{mn}}{R}, \tag{2.11}$$

$$E_0 = \sqrt{\frac{\mu}{\epsilon}}\frac{k_1}{k}, \tag{2.12}$$

$$E_r = -\frac{k_3}{k_1}E_0 J'_m(k_1 r)\cos(m\varphi)\sin(k_3 z), \tag{2.13}$$

$$E_\varphi = \frac{mk_3}{k_1}E_0\frac{J_m(k_1 r)}{k_1 r}\sin(m\varphi)\sin(k_3 z), \tag{2.14}$$

$$E_z = E_0 J_m(k_1 r)\cos(m\varphi)\cos(k_3 z). \tag{2.15}$$

TE modes:

$$k_1 = \frac{x'_{mn}}{R}, \tag{2.16}$$

$$E_0 = -\sqrt{\frac{\mu}{\epsilon}}, \tag{2.17}$$

$$E_r = E_0 m\frac{J_m(k_1 r)}{k_1 r}\sin(m\varphi)\sin(k_3 z), \tag{2.18}$$

$$E_\varphi = E_0 J'_m(k_1 r)\cos(m\varphi)\sin(k_3 z), \tag{2.19}$$

$$E_z = 0. \tag{2.20}$$

In equations 2.8 to 2.20, μ is the magnetic permeability of the medium in the cavity and ϵ is the absolute permittivity of the medium inside. When the resonance frequencies in vacuum are calculated $\mu = \mu_0$ and $\epsilon = \epsilon_0$, so that $\frac{1}{\sqrt{\mu_0\epsilon_0}}$ reduces to the speed of light c.
The symbol x_{mn} denotes the n-th zero of the m-th Bessel function ($J_m(x) = 0$) and x'_{mn} is the n-th zero of the derivative of the m-th Bessel function. The equations have three indices, m, n and p, because the cavity is three-dimensional. These indices can have the following values:

$$m = 0,1,2... \;\; n = 1,2,3... \;\; p = 0,1,2...$$

For TE modes p can not be equal to zero. The modes can now be written as TM_{mnp} or TE_{mnp}. The resonance frequency for both TM and TE can be calculated according to:

$$f = \frac{k}{2\pi\sqrt{\mu\epsilon}}. \tag{2.21}$$

Figures 2.3 and 2.4 show the oscillations of the electromagnetic field of TM modes in a cylindrical cavity. These oscillations are standing waves, which means that there will only be movement in the vertical direction. These pictures can also be made for $p>0$, but it will be more difficult because p will change all three components of the electric field.

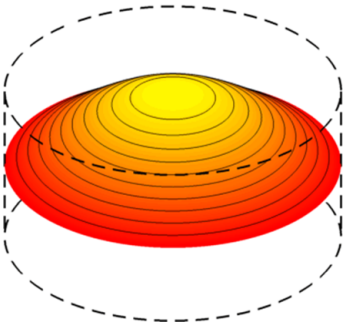

Figure 2.3: *TM010.*

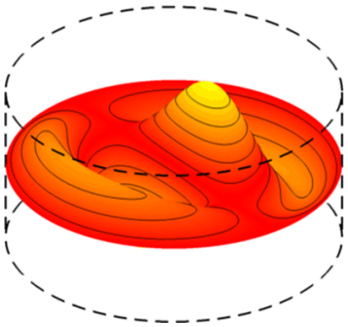

Figure 2.4: *TM120.*

2.4.1 Frequency shift

When the cavity is filled with a medium other than vacuum or air, an argon plasma for example, the resonance frequency will shift. As a (good) approximation we take $\mu = \mu_0$, whereas ϵ will change due to the presence of plasma (free electrons). When the resonance spectrum of a cavity is measured, there will be some differences between the spectrum in vacuum and with a active plasma. The resonance spectrum with the plasma will show that some peaks are shifted to the right due to a change in medium permittivity, caused by a change in electron density. The electron density is given by

$$n_e = \frac{8\pi^2 m_e \epsilon_0 f^2 \Delta f}{e^2 f_0}, \tag{2.22}$$

with n_e the averaged electron density, m_e the (rest) mass of an electron, ϵ_0 the electric permittivity of vacuum, e the elementary charge, Δf the frequency shift, f_0 the resonance frequency without an active plasma and f the resonance frequency when the plasma is turned on.

3 Experimental Setup and Methods

3.1 Parameter study

3.1.1 Setup

The setup used to do a parameter study of a dusty plasma is schematically shown in figure 3.1. The picture shows a cavity mounted inside a vacuum vessel. A mixture of Ar and C_2H_2 enters the cavity through a shower head from the top. Both gas flows can be adjusted using mass flow controllers (Brooks Model 5850E). The upper plate of the cavity serves as the powered electrode for the plasma. The side wall of the cavity is a metal mesh (thread width 0.35 mm, mesh size 1.06 mm, translucency 57%), so it possible to look into the cavity. The voltage applied to the upper electrode and the pressure inside the vessel can also be varied.

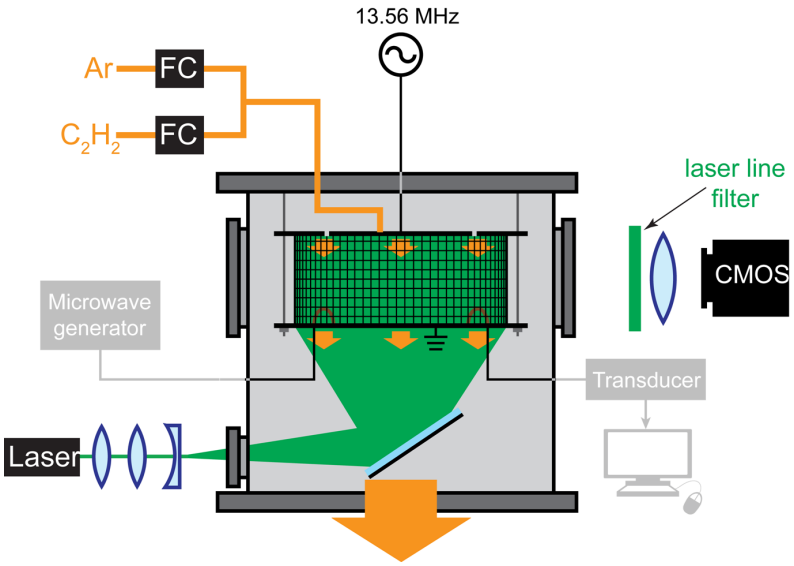

Figure 3.1: *Setup with mirror.*

The function generator (Rigol DG1022) is set at a frequency of 13.56 MHz, but it does not have enough power to drive the plasma, so an amplifier (Amplifier Research Model 75A250) is used to amplify the signal. The Smart PIM (Scientif System Serial No. 0042501) is used to measure the current, voltage, phase, power and impedance, but we will only look at the phase and power of the plasma. Especially the power and phase give insight in the periodic dust particle formation and therefore also in the development of the dust void.
A video camera is placed outside the vessel and is aimed at the cavity. With this camera the dust particles inside cavity will be recorded. But before they can be filmed, they have to be made visible. This is done with the help of a laser. The laser light will first go through a series of lenses. A cylindrical lens turns the laser beam line into a laser light plane. Subsequently, the light enters the vessel via the bottom flange and reflects on a mirror. The light will enter the cavity via a slit in the bottom plate (see figure 3.2). The laser light will scatter if there are dust particles in the cavity. This scattered light is filmed by the camera. Please note that, for clarity, the placement of the camera is not correctly shown in figure 3.1, because it is actually placed in front of the vessel, which means that the camera has a 90 degree angle with the scattering plane.
An optical filter that transmits light of 532 nm with a FWHM of 10 nm is put in front of the camera to make sure that the camera only records the scattered laser light. The microwave generator and transducer are not used in this experiment and will be explained later on.

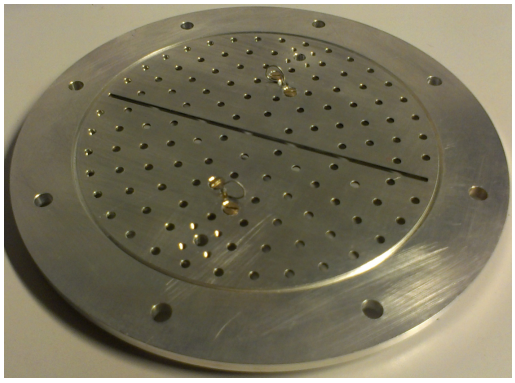

Figure 3.2: *Bottom plate of the cavity with the slit in the center.*

The setup has been slightly changed when the parameter study was about half way. This means that half of the measurements are done with the new setup. The mirror has been removed and the laser and lenses are now put at the same height as the cavity. The laser light now reaches the cavity without reflection.
The change in the setup will not have an impact on the experiment, only the videos from the camera will be a bit different. The light intensity will be higher at the sides of the cavity because of the reflections on the metal mesh and the side of vessel and there will be less loss of light without the reflection on the mirror.

3.1.2 Method

For these measurements the amplitude of the signal and the pressure inside the vessel are constant. The amplitude is set to 90 mVpp (this is before the signal reaches the amplifier, corresponding to about 5-9 W of dissipated power) and the pressure is kept at 0.2 mbar (= 20 Pa). For this parameter study, the gas flow for the Ar- and C_2H_2-gas are varied.
Recording of the video and plasma-dissipated power and phase angele starts when the plasma has been running for a few minutes, depending on experimental conditions. The measurement does not start immediately because there are no dust particles present in the cavity. The dust particles have to be created first before a void can appear in the dusty plasma. This is important because for this study the void is our focus point.
For each experiment, the electric parameter of the plasma are recorded with the Smart PIM and the laser light scattering on the dust particles is recorded with the video camera. When a measurement is completed, the plasma will be turned off and the gas flows will be stopped. The remaining gas will be pumped out of the vessel so that the cavity is in vacuum again. After that the new settings are applied and, when the pressure is at 0.2 mbar, the plasma is turned on again.
The videos of the plasma are analysed together with the graphs made with the data. For each new setting the shape of the void is determined and depending on the shape a certain color code is assigned to those settings.
The goal of this experiment is to determine the influence of the gas flows of argon and acetylene on the void in the dusty plasma. A change in the gas flow can influence the growth of the particles (section 2.2.2) in such a way that there a more or bigger particles, altering the force balance. This will also have an effect on the shape of the void.

3.2 Microwave resonance measurements

3.2.1 Setup

To measure the resonance spectrum of the cavity, some additional equipment is needed. Figure 3.3 shows a schematic representation of the new setup. The laser, camera, RF-generator and the gas supply are not necessary for this experiment and the microwave generator (Gigatronics 605) and transducer (Agilent 8470B crystal detector) are added to the setup. Inside the cavity two (copper) antennas are placed. The computer-controlled microwave generator is connected to one of the antennas. The resonance frequency is obtained by sweeping the applied frequency from 2 GHz to 8 GHz with steps of 1000 kHz.
The second antenna is connected to an ADC (TRC100 within a TUeDACS/6 system), which converts the signal from the antenna so the data can be stored on the computer. When the measurement is done, the resonance spectrum can be made with the help of a Matlab script.

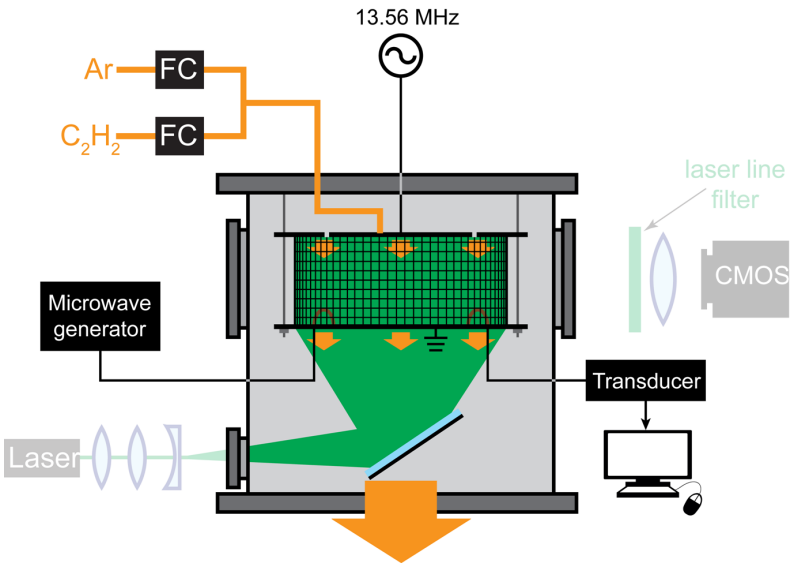

Figure 3.3: *Setup for the resonance measurements.*

The antennas are not just randomly placed in the cavity. They are positioned such that, in theory, it would be the best location to only excite the TE_{0xy} modes. Only these modes can be excited due the geometry of the cavity. According to equations 2.18 and 2.20 E_r and E_z are both equal to zero for these modes, which means that the electric field lines are azimuthal. The magnetic field lines are in the r and z direction. The magnetic field and field lines for TE_{011} are shown in figures 3.4. If one wants to excite a different mode the picture can change drastically, as for instance for TM_{010} for which the field lines are shown in figure 3.5. Now the best location and orientation for the antennas are as shown in the figure, where (again) the magnetic field is maximal. The magnetic field is at its maximum at about 70% of the radius.

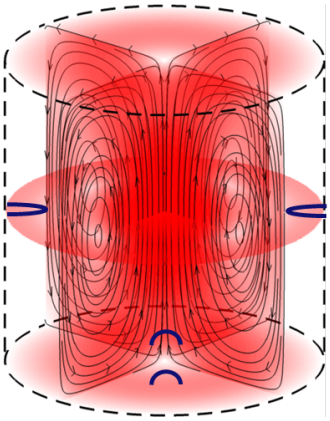

Figure 3.4: *Magnitude of the magnetic field (scaling with the intensity of the color red) and the corresponding field lines (black with arrows) for TE_{011}.*

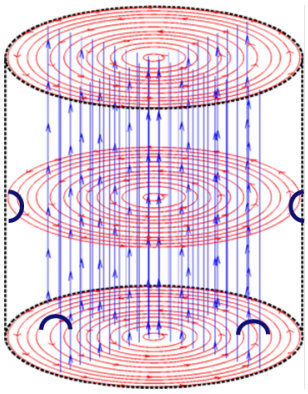

Figure 3.5: *Blue = electric field lines, red = magnetic field lines for mode TM_{010}*

The best locations for excitation of the TE modes are at the bottom plate or at the side of the cavity (figure 3.6), but the antennas can not be placed at the side because of the metal mesh. Thus only one location remains. The antennas have to be formed as a loop with its plane normal to the magnetic field lines and they have to be placed at a maximum of the field in order to properly excite the TE modes (figure 3.7). The antennas are placed 32.5 mm away from the center so that they are at the maximum of the field.

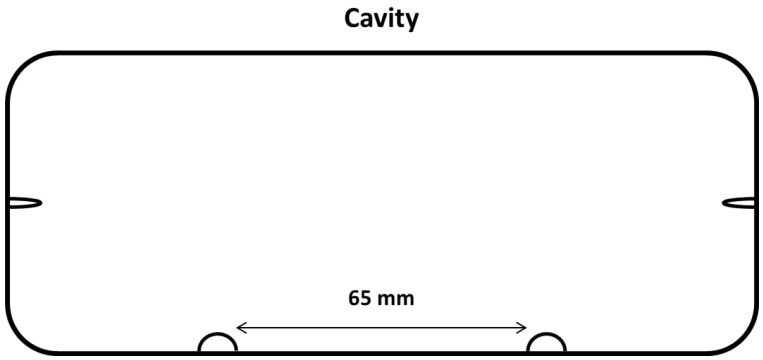

Figure 3.6: *Two options for optimal placement of the antennas inside the cavity. For practical reasons, the antennas in the bottom plate are used, see text.*

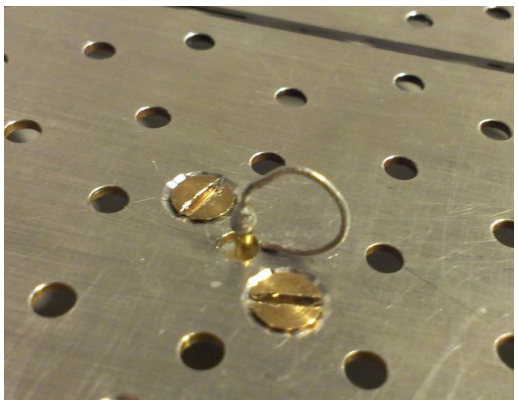

Figure 3.7: *One of the two antennas attached to the bottom plate of the cavity. Note that the slit for the laser light plane is visible in the top right portion of the photograph.*

3.2.2 Methods

The resonance spectrum of the cavity is measured in two ways: 1) when the vessel is still at vacuum conditions and 2) when an argon plasma is switched on in the cavity. The height of the cavity is also varied, the first measurements are done with a cavity a height of 40±0.5 mm, the second measurement with a height of 30±0.5 mm. The diameter is 135±2 mm. The spectrum of the vacuum and the plasma are compared with each other. Furthermore, the spectra will be used to determine which modes, TE and TM, can be found in the cavity. The frequencies of the modes can be calculated with the equations of chapter 2.4.

4 Results and Discussion

4.1 Parameter study

As stated in the experimental setup, the pressure and the plasma-dissipated power are kept constant at every measurement. The gas flow of argon and acetylene is varied. For this experiment a cavity with a height of 40 mm is used.

4.1.1 General observations

When the plasma is ignited, the plasma will fill with particles up to micrometer sizes. These particles will levitate inside the cavity and a void can appear. But the void does not stay at a certain size, it will grow. Several seconds later, the expansion stops and the void even shrinks for a brief moment. It will resume to expand thereafter. This process is called the hiccup. The hiccup is caused by coagulation of a new group of dust particles inside the void. This process is periodical and reproducible (figure 4.1.

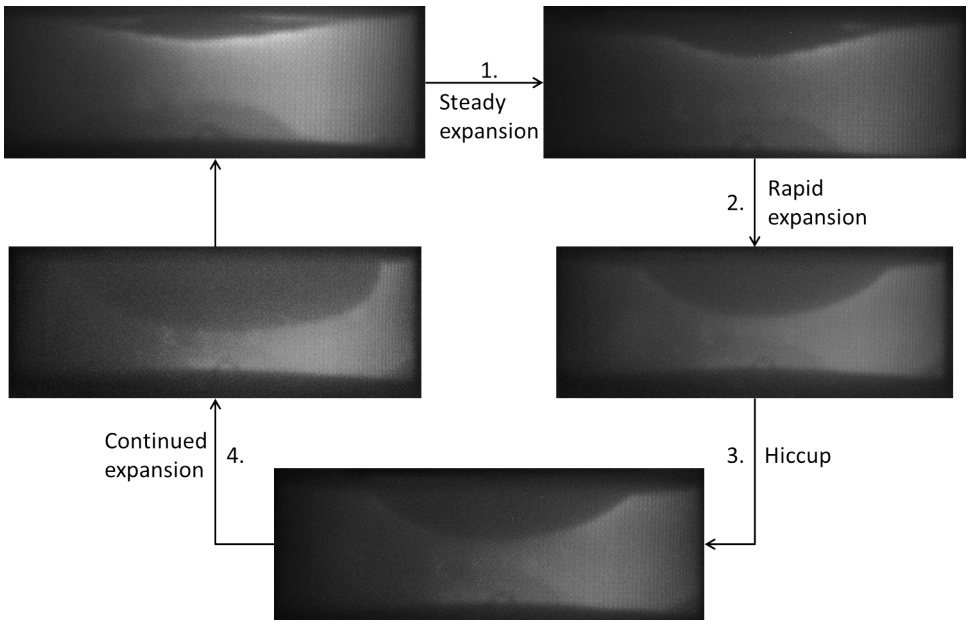

Figure 4.1: *Cyclic behaviour of the dust void expansion.*

4.1.2 Color code

A video of the laser light scattering is made for every new setting. Each video is analysed to see if a void is created in the plasma. If there is a void, the shape of the void will be analysed as well. Each experimental setting is assigned to a code which corresponds with the type of void observed in the plasma. The different shapes of the voids are divided into four classes: the ('perfect') ellipsoidal void (color code green), the ellipsoidal void with random discharges (color code orange), the tornado-shaped void (color code yellow) and no void (color code red). Some examples of these types of voids are shown in figures 4.2 to 4.4.

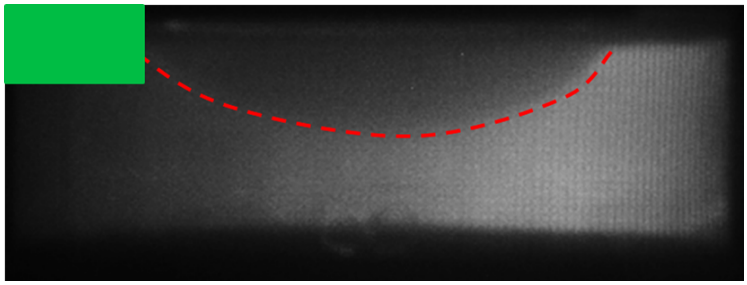

Figure 4.2: *An ellipsoidal void.*

A video will have the color code green when an ellipsoidal void in the plasma is observed and there are no random discharges or turbulent streams in the plasma. This type of void also has a periodic cycle and hiccup as mentioned before.

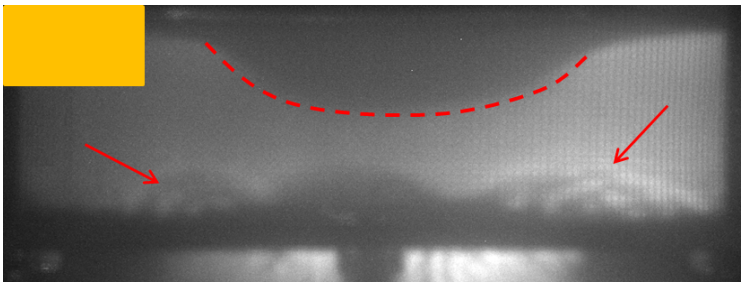

Figure 4.3: *An ellipsoidal void with random discharges at the bottom of the cavity.*

Picture 4.3 shows some random discharges at the bottom of the cavity (indicated with the arrows). If this event is observed and the void has an ellipsoidal shape it will get the color code orange.

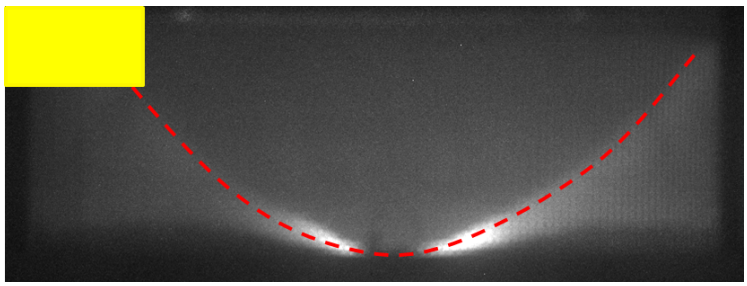

Figure 4.4: *A tornado-shaped void.*

Sometimes the void had such a shape, that it would reach the bottom plate of the cavity. It does not have a periodic cycle and no hiccup. The void maintains the tornado-shape all the time. This type of void has color code yellow.

A graph of the phase and power of the plasma has been made with the help of the PIM software. Unfortunately these graphs do not give a clear insight in the type of void inside the dusty plasma, but do show the periodicity (if present) quite clearly. Graphs for an orange or yellow void do not show any periodicity in the power. The phase does show some periodicity, but the height of the peaks differs more than the peaks in a graph with the green color code. For a green void both the phase and power are periodic. The height of the peaks stays almost the same each period too.
The graphs are not very useful to determine the shape of the void, but they are useful to confirm if the green color code is applied correctly. Some typical graphs are shown below.

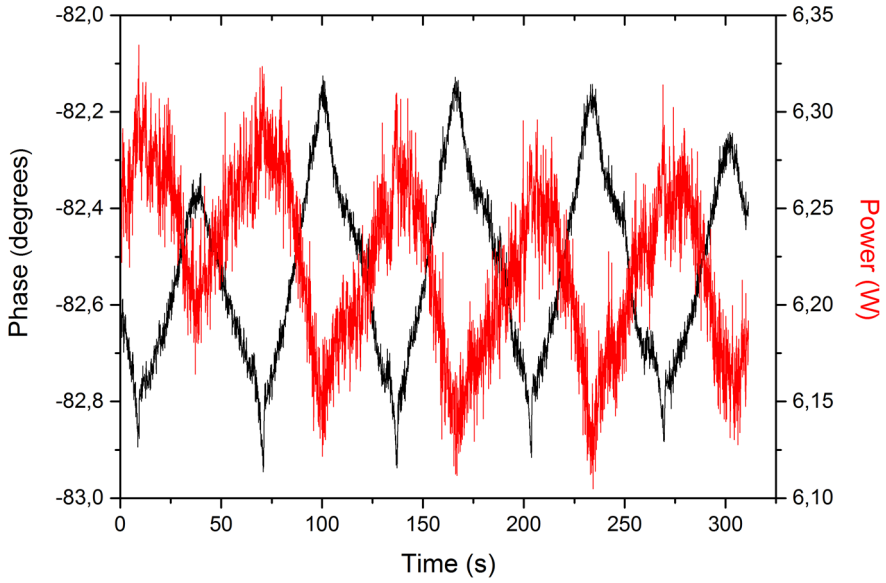

Figure 4.5: *Phase and power against time for a void with color code green.*

The graph for a measurement with color code green (figure 4.5) shows that the phase and the power both are periodic. In some cases, it is even possible to see when the hiccup occurs.
The graph with color code orange (figure 4.6) does show some periodical behaviour in the power. The power is at its maximum when the phase is at its minimum and vice versa, but the measurement contains a lot of noise. This is probably due to the random discharges at the bottom plate of the cavity. The phase does look periodic, but the amplitude starts to shrink during the measurement. The yellow color code void had similar graphs (figure 4.7).

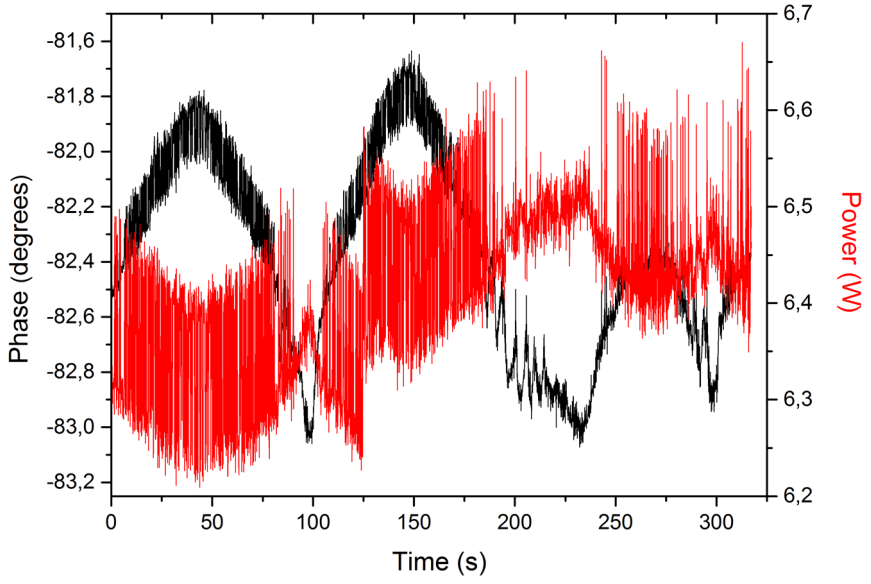

Figure 4.6: *Phase and power against time for a void with color code orange.*

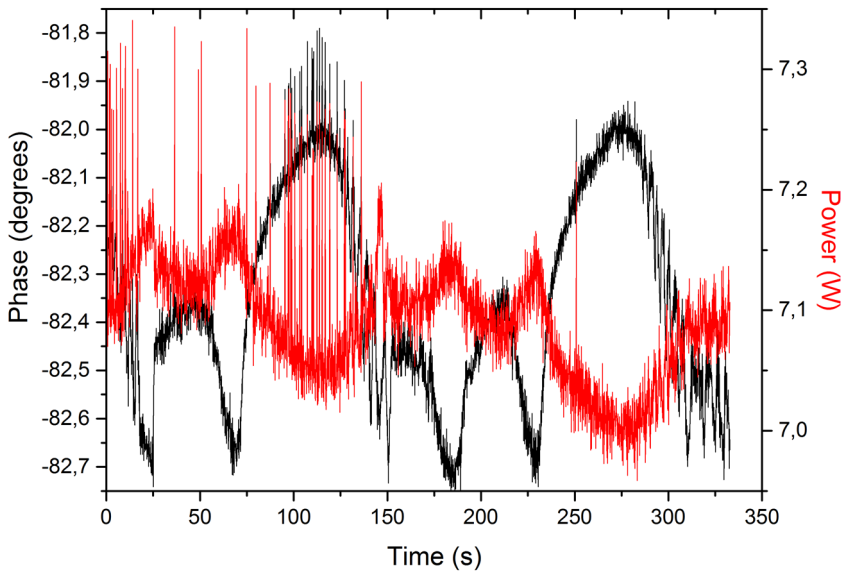

Figure 4.7: *Phase and power against time for a void with color code yellow.*

However, in this graph it looks like the power is periodic as well. Unfortunately this was not the case for the other yellow voids. Thus by only looking at the periodicity of the power it is impossible to determine if the void should get the green or yellow color code. This proves that the graphs are not accurate enough to determine the shape of the void.

4.1.3 Influence of the gas flows on the shape of the void

After analysing all videos, a table is made where the acetylene gas flow is set against the argon gas flow with the corresponding color code. The results are shown in figure 4.8. The gas flow could be adjusted via the computer, and for the measurements they ranged from 1-3.5 sccm (standard cubic centimeters per minute). However, these values are not the real values of the gas flow. After calibration measurement the real flow values have been calculated for both gasses. The real flow values are used in figure 4.8.

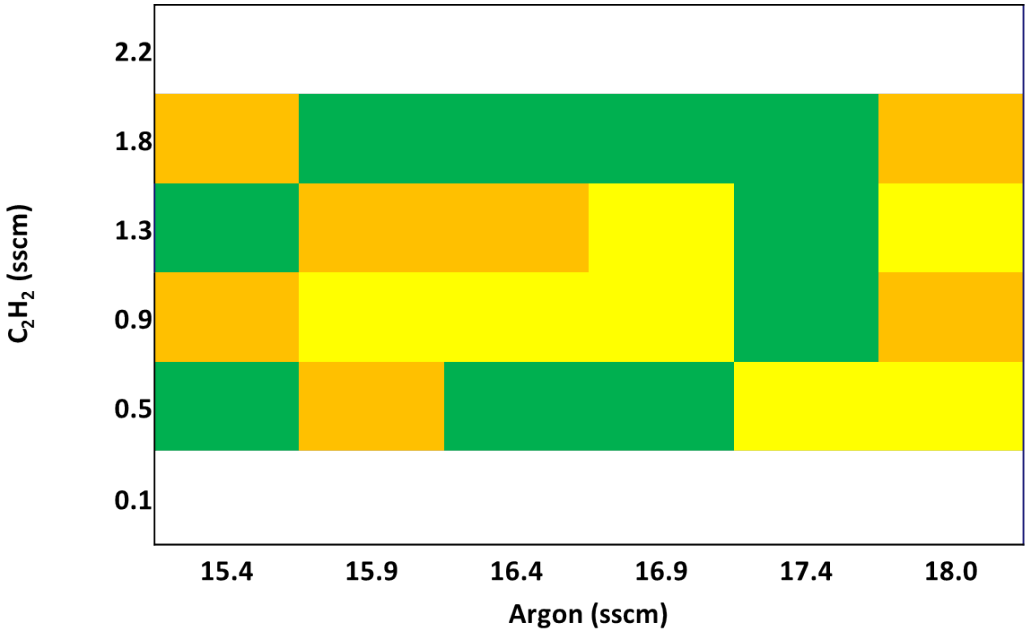

Figure 4.8: *Acetylene gas flow against the argon gas flow and corresponding color code.*

This result does not give a clear insight in the influence of the gas flows on the shape of the void, because if one of the gas flows changes a little, the shape of the void can change a lot. For example if the C_2H_2 flow is at 0.9 sccm and the argon flow is somewhere between 16.9 and 17.4 sccm the shape of the void can be ellipsoidal or tornado like. This means that there is not a real transition from an ellipsoidal void to a tornado-shaped void due to change in the gas flow. So to get a better insight the ratio (C_2H_2/Ar) of the two gas flows is calculated and sorted from low to high with corresponding color code. See figure 4.9.

0.0293	0.0749
0.0302	0.0771
0.0312	0.0795
0.0321	0.0821
0.0332	0.0848
0.0343	0.0877
0.0521	0.0977
0.0537	0.101
0.0553	0.104
0.0571	0.107
0.0590	0.111
0.0610	0.114

Figure 4.9: *Ratios sorted from low to high.*

This table shows that there are some regions where it is possible to create an ellipsoidal void (0.031-0.053 and 0.082-0.111) and there are regions where only tornado-shaped voids will appear (0.055-0.059). So as long as the ratios are kept at a certain value it is very likely that a void, corresponding with its color code, is observed. This means that value of both gas flows does not determine the shape of the void, but it depends on the ratio of both flows. As long as the ratio stays the same, the shape of the void will not change.

If this parameter study is done again it is very likely that one gets the same results with these conditions. Some of the measurements were done again a few days later. These measurements were all done at the same day and about 70 to 80 percent gave the same result as before. However, for some voids it is possible to give them an other color code, because the coding depends on the interpretation of the researcher. For example, if in a video of an ellipsoidal void some random discharges occur for a brief moment and then never appear again, one can give the video the color orange and the other may give the color green.

4.2 Microwave resonance

4.2.1 Comparison

The microwave resonance spectrum (at vacuum) was measured previously with cavities with a height of 30 and 40 mm (figure 4.10), but these measurements were done without paying much attention to the antenna configuration. In this research, the antennas are placed in the configuration explained in section 3.2.1. The resonance spectrum is measured again (figure 4.11) for both cavities and compared with the old spectrum.

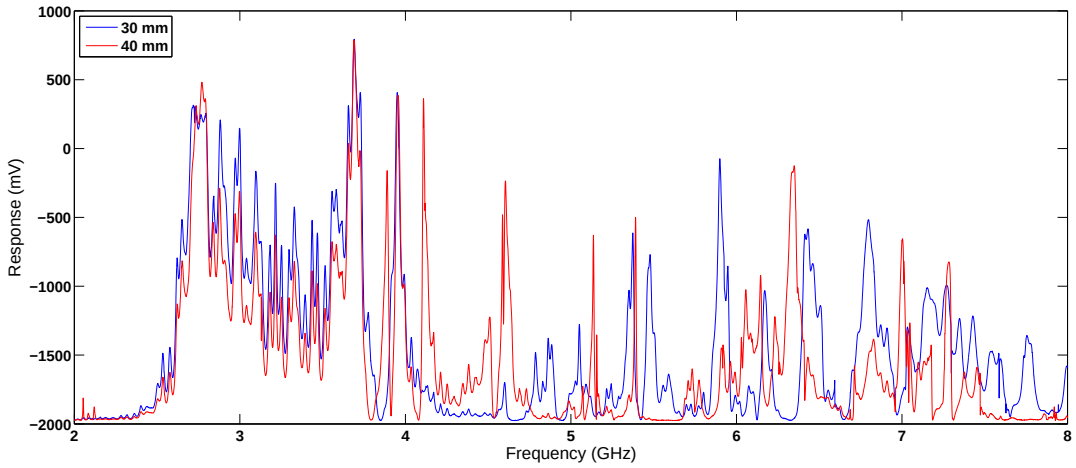

Figure 4.10: *Old spectrum.*

The vertical axis shows the measured response in mV (as obtained by the ADC, see section 3.2.1) and the horizontal axis shows the frequency ranging from 2 to 8 GHz.

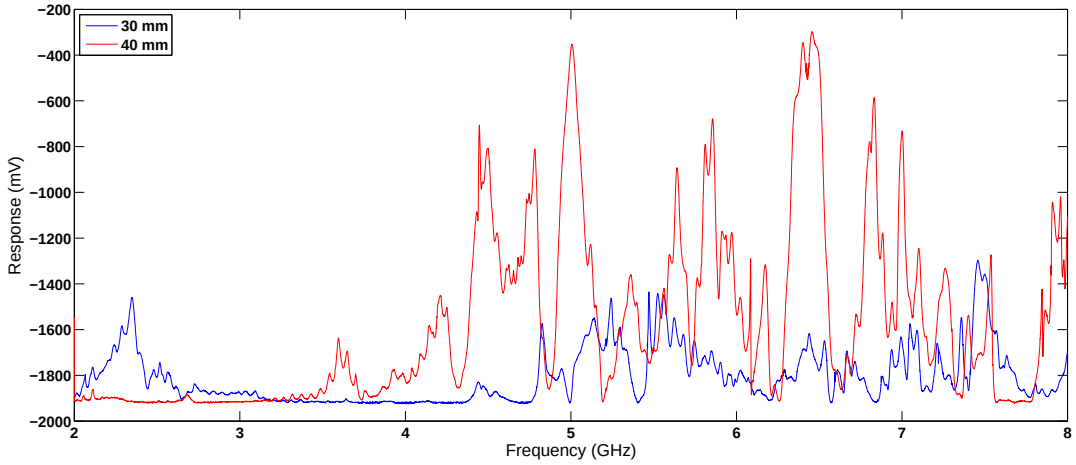

Figure 4.11: *New spectrum.*

The new spectra contain less peaks than the old spectra, especially in the range from 2 to 4 GHz. The other peaks in the new spectrum also appear to be wider and not a sharp as in the old measurement. The graph for the cavity with a height of 30 mm has a much lower response than the 40 mm cavity.

This is probably due to the configuration of the cavity inside the vessel. The two plates of the cavity are pressed on the metal mesh. When the plates are pressed too hard on the metal mesh it will slightly bend outwards, thus changing the shape of the cavity. The cavity was not ideal already due to the holes in the walls, but now it is less cylindrical as well. This will influence the coupling of the emitted EM waves and therefore the measured response.

4.2.2 Frequency shift and excited modes

Next, the resonance spectra are also measured when an argon plasma is active. These spectra are compared with the spectra at vacuum. It is also investigated which TE or TM mode could have been excited during the measurement. Figures 4.12, 4.15, 4.16 and 4.17 show the spectra for the 30 an 40 mm cavities, with the first two graphs showing the TE_{mnp} modes and the last two the TM_{mnp} modes which fit in the 2-8 GHz range. If a frequency of a TE_{0xy} mode corresponds to a peak in the vacuum spectrum it is very likely that the modes was excited. The graphs are made with a Matlab script (A.1) in which the radius and height of the cavity can be changed.

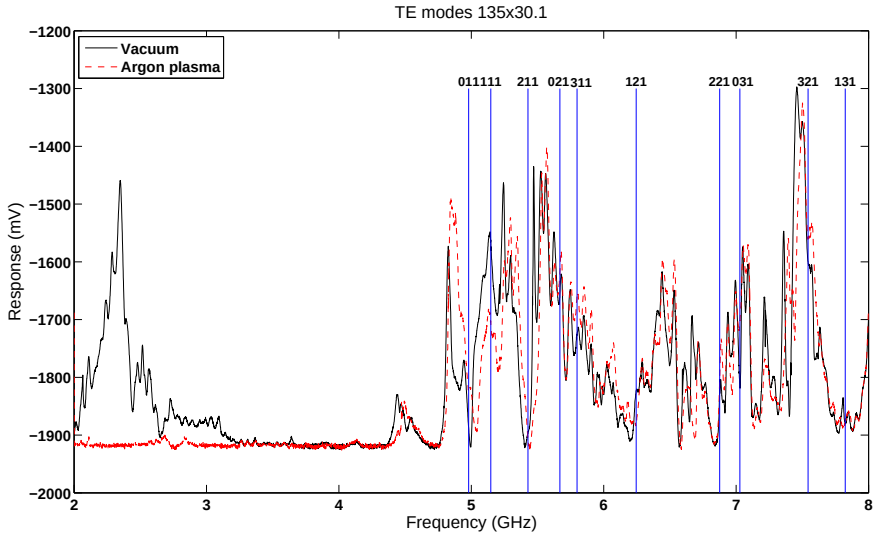

Figure 4.12: *TE modes for the 30 mm cavity.*

The first thing that stands out is the disappearance of the peak at 2.4 GHz due to the presence of the plasma. Apparently the plasma shields off these frequencies, so it is very likely that these frequencies are not resonance frequencies of the cavity. Perhaps these frequencies are generated in the cables or outside the vessel. Some other peaks are shifted to the right. The size of the shift differs between 0 and 50 MHz. The peak at 5.25 GHz has a shift of 50 MHz. Equation 2.22 gives an (averaged) electron density of 6.45e15 m^{-3}.
Although the antennas are put in such a configuration that, in theory, the TE_{0xy} modes should be excited, this is not the case. It is impossible for the TE modes to have a complete overlap with the spectrum for one set of dimensions of the cavity. Some peaks do correspond to the theoretic model, for example TE_{111} and TE_{021}, and other peaks do not (for example TE_{011}). Unfortunately, this was to be expected and inevitable. The main reason why is because the cavity is far from ideal and so are the field patterns of the resonances. This changes the resonance frequency and does not correspond with the theoretical value of the perfect cylinder any more.
The dimensions in the theoretical calculation are adjusted to make sure that the best possible correspondence is found. Peaks which differ several dozen MHz with the theoretical value can represent that resonance and they probably will.

When calculating the frequencies of the modes, the dimensions of the cavity have been varied within the error range. As said before, the cavity is not perfect and the height can be different because of the deformation of the metal mesh. For this measurement, the modes showed the most correspondence with the resonance spectrum when the dimensions of the cavity were 135 by 30.1 mm.

To illustrate the influence of the numerical values of the radius and height on the resonant frequency, the calculations for TE_{011} and TE_{021} are also done for different values of radius and height (figures 4.13 and 4.14).

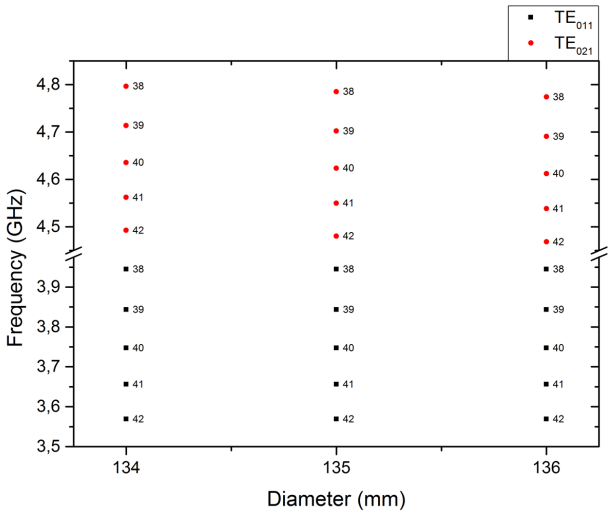

Figure 4.13: *Influence of the diameter on the resonant frequency. The number next to a data point is the height of the cavity in mm.*

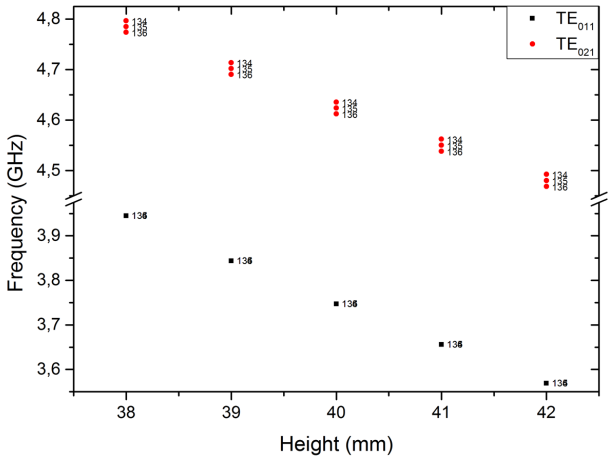

Figure 4.14: *Influence of the height on the frequency. The number at a data point is the radius in mm.*

These graphs show that a change in height has a bigger impact on the resonant frequency than a in change in the radius.

Next, the resonance spectrum of the 40 mm cavity is measured with an without an active plasma. See figure 4.15.

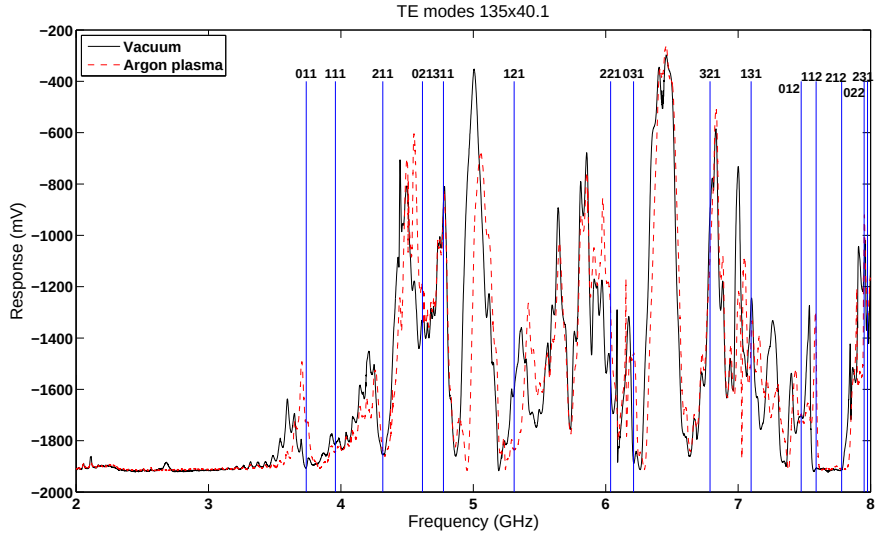

Figure 4.15: *TE modes for the 40 mm cavity.*

The resonance spectrum with an active plasma in the bigger cavity only shows some peaks that have shifted to the right. The size of these shifts is somewhere between 0 and 60 MHz. The peak at 5.36 GHz shifted 60 MHz to the right when the a plasma was active. Here, the electron density is equal to 7.89e15 m^{-3}.
For this cavity the modes showed the most correspondence when the dimension were 135 by 40.1 mm. Please note that these dimensions are also used for the TM modes below, because it is the same spectrum. This does not guarantee the best correspondence for the TM modes, because every mode reacts differently on the imperfections. However, it is 'fair' to keep the dimensions the same for these modes.
For the modes that should, theoretically, be most efficiently excited, TE_{0xy}, only TE_{021} and TE_{022} seem to have a relative high response (-1300 mV and -1100 mV respectively). The other TE_{0xy} modes all have a low response, which makes it very unlikely that they have been excited efficiently. Some other modes which apparently are efficiently excited are $TE_{311,\ 131}$.

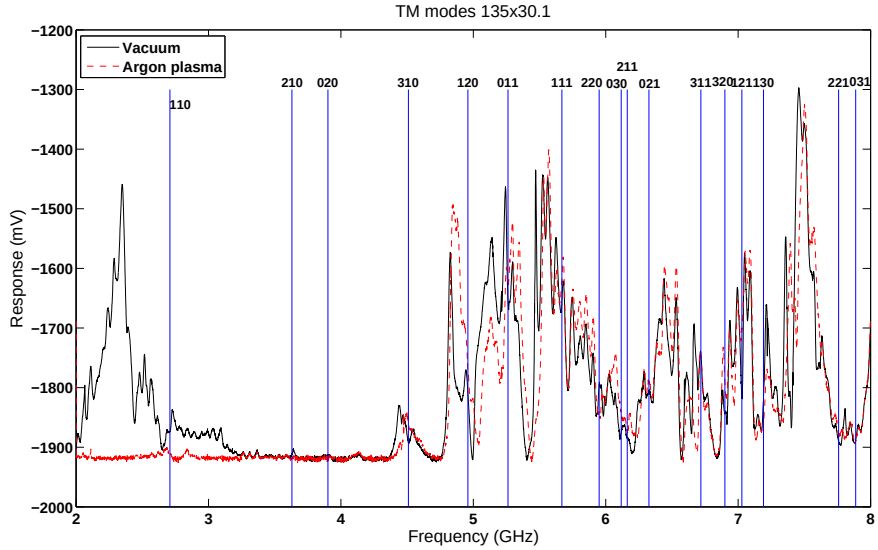

Figure 4.16: *TM modes for the 30 mm cavity.*

According to section 3.2.1, TM modes cannot efficiently be excited, but that is only the case under ideal circumstances (i.e. a perfect cavity). It appears that some modes have been excited, for example $TM_{110,\ 210,\ 111,\ 311}$. This is also the case for the 40 mm cavity (figure 4.17).

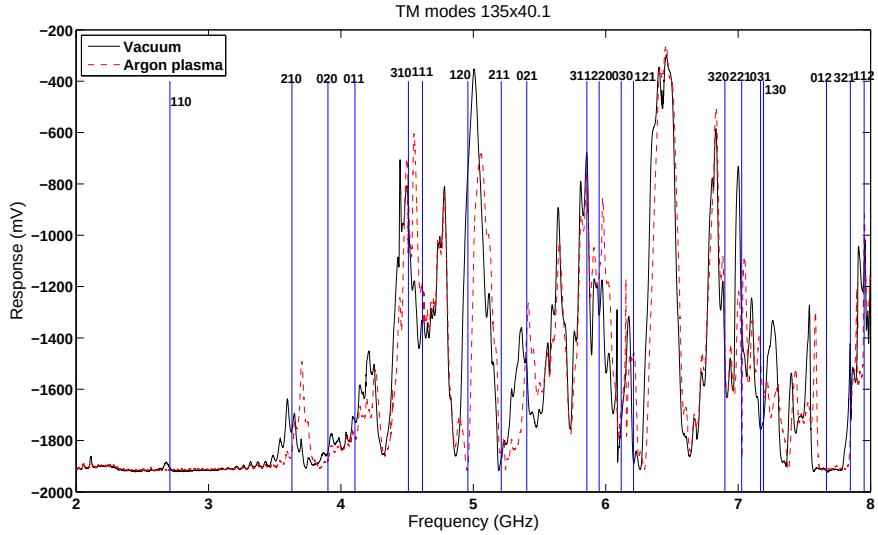

Figure 4.17: *TM modes for the 40 mm cavity.*

Again, it looks like some modes have been excited. Modes like $TM_{111,\ 311,\ 321}$. So it looks like there are some TM modes excited even though we did not expect them. Perhaps the TM modes are easier to excite than the TE modes for reasons unknown to us at this point.
After all the measurements we can conclude that it is very difficult to link a measured spectrum to a theoretical spectrum of an ideal closed cavity. First of all, the cavity is not closed because the metal mesh and the holes in the bottom plate. Second, the metal mesh can deform when the plates of the cavity are pressed too hard on the metal mesh, which makes the cavity less cylindrical as well.

5 Conclusion and recommendations

5.1 Parameter study

The hypothesis was that changing the absolute flows of argon and acetylene would change the shape of the void. and that this would be somehow related to the changing forces. The shape of the void can be different as a result of a different particle growth cycle, resulting in particles of different size and shape. This alters the force balance, but the changing gas supply alters the forces as well, the neutral drag force in particular. The voids are divided in three categories: ellipsoidal, ellipsoidal with random discharges and tornado-shaped. This did not show a clear trend when looking at absolute flow values. However, looking at the ratio of the argon and acetylene flow does show a trend and, generally, the type of void is a function of this ratio. In other words, changing the absolute flow values, but keeping the gas flow ratio constant does not change the type of void. However, the generality of this rule/observation holds only within certain limits of the gas flows. Furthermore, void formation was always observed for every measurement.

5.2 Microwave resonance

The new microwave resonance spectra contain fewer peaks thanks to the new antenna configuration and they show a lot of different modes. A cavity with a solid metal wall would probably show less modes. It proved to be difficult to match/link theoretical modes with measured resonant peaks. Contrary to our expectations, TM modes showed up in the spectrum. Better correspondence was found between the measured spectrum and the TM modes, than with the TE modes. The TM modes are probably easier to excite than the TE modes.
It looks like that for both cavities TE_{021} is excited efficiently and for each cavity some other modes as well. These modes and every shifted peak can be used to calculate the electron density. For these calculations it would be nice if the field distribution is known, but this research and a previous study [3] show that the only method to do this is to actually measure the field.

5.3 Recommendations and future experiments

For future experiments one could try to vary the pressure and plasma-dissipated power instead of the gas flow and investigate the influence of this on the shape of the void and look for a correlation between the two variables. It is also possible to try to explain the shape of the void due to the change of the gas flows with a mathematical model, but this is very challenging! The setup can be improved in several ways. First the laser alignment can be made more stable, because it now is very easy to shift the laser with a small touch. A second improvement would be a gas flow from the bottom of the cavity. This could ensure a much more stable plasma as well as flip the neutral drag force, which then competes instead of assists gravity. This could result in bigger dust particles sizes (and confinement times).
For further research it would be interesting to look at the time it takes for the particles to form at certain settings, but also at the time it takes for the void to be created and the time of one cycle of the void.
To improve the microwave resonance spectrum measurement and get a better insight in the excited modes, the cavity should be fully closed, but this would make it impossible for the gas to enter or leave the cavity. Only a solid wall looks like a logical solution, because the gas can still enter and leave the cavity, but it is not preferred because the plasma and dust particles cannot be seen. When it is clear which modes are excited in the cavity they can be used to determine more accurately the electron density inside the cavity, which when using MCRS always is a field-weighted value.

Reference list

[1] J.Goree, G.E. Morfill, V.N. Tsytovich and S.V. Vladimirov. *Theory of dust voids in plasmas*, 1999.

[2] F.M.J.H. van de Wetering. *Ethynyl anion (C_2H^-) dynamics in the first 10 milliseconds of an argon-acetylene radio-frequency plasma*, Master's thesis, Eindhoven University of Technology, 2011

[3] R.J.C. Brooimans. *Spatiotemporal characterization of dust-forming acytelene plasma*, Traineeship report, Eindhoven University of Technology, 2014.

[4] J. Beckers. *Dust particle(s) (as) diagnostics in plasmas*, PhD thesis, Eindhoven University of Technology, 2011.

[5] Robert L. Merlino. *Plasma Physics Applied, Chapter 5*, ISBN: 81-7895-230-0, 2006.

[6] Andre Melzer and John Goree. *Fundamentals of Dusty Plasmas.*

[7] D.J. Griffiths. *Introduction to Electrodynamics*, Addison Wesley, 5th edition, 2014.

[8] K. De Bleecker, A. Bogaerts, and W. Goedheer *Detailed modeling of hydrocarbon nanoparticle nucleation in acetylene discharges*, 2006

[9] K. De Bleecker, A. Bogaerts, and W. Goedheer. *Numerical investigation of particle formation mechanisms in silane discharges*, 2004

[10] K. De Bleecker, A. Bogaerts, and W. Goedheer. *Modeling of the formation and transport of nanoparticles in silane plasmas*, 2004

A Matlab

A.1 Plot a graph of the spectra and modes.

```
function SpectrumModes(Data1, Data2, Data3, Data4, indexToPlot, R, d1, d2)
% R is the radius of both cavities, d1 is the height of the cavity ...
    corresponding to the cavity used for
% Data1 and Data 3, d2 is the height of the cavity corresponding to the cavity ...
    used for Data2 and Data 4.
% R, d1 and d2 have to be given in m! All frequencies are in GHz.
% If only one cavity is used, Data 2, Data 4 and d2 can be eliminated from the ...
    function input.

files_1 = dir([Data1 '\*.dat']);        %Vacuum, 40 mm
nFiles_1 = length(files_1);
files_2 = dir([Data2 '\*.dat']);        %Vacuum, 30 mm
nFiles_2 = length(files_2);
files_3 = dir([Data3 '\*.dat']);        %Argon, 40 mm
nFiles_3 = length(files_3);
files_4 = dir([Data4 '\*.dat']);        %Argon, 30 mm
nFiles_4 = length(files_4);

%%Construct the spectra
for k = 1:nFiles_1
    fileName_1 = files_1(k).name;
    Path_1 = fullfile(Data1,fileName_1);
    rawData1 = load(Path_1);
    data1CH0(:,k) = rawData1(:,1);
    Vector_1(k) = str2double(fileName_1(1:end-4));
end

for k = 1:nFiles_2
    fileName_2 = files_2(k).name;
    Path_2 = fullfile(Data2,fileName_2);
    rawData2 = load(Path_2);
    data2CH0(:,k) = rawData2(:,1);
    Vector_2(k) = str2double(fileName_2(1:end-4));
end

for k = 1:nFiles_3
    fileName_3 = files_3(k).name;
    Path_3 = fullfile(Data3,fileName_3);
    rawData3 = load(Path_3);
    data3CH0(:,k) = rawData3(:,1);
    Vector_3(k) = str2double(fileName_3(1:end-4));
end

for k = 1:nFiles_4
    fileName_4 = files_4(k).name;
    Path_4 = fullfile(Data4,fileName_4);
    rawData4 = load(Path_4);
    data4CH0(:,k) = rawData4(:,1);
    Vector_4(k) = str2double(fileName_4(1:end-4));
end

%%Calculate the frequencies for the first cavity (R,d1)
A=[];
i=1;

%TM
for m = 0:3
    for n = 1:2
        for p = 0:2
            x_mn = zerobess('J',m,n); % Calulate the first n zeros of the ...
                Bessel function of the first kind: J_m(x) = 0
            x_mn = x_mn(end); % We are interested in n-th zero, this being the ...
                last value of the vector x_mn
```

```
59              freq = (299792458/(2*pi))*sqrt(x_mn^2/R^2+p^2*pi^2/d1^2); % ...
                    Calculate the actual frequency in Hz
60              freqGHz = freq*1e-9;
61              A(i,1)= m*100+n*10+p;
62              A(i,2)= freqGHz;
63              i=i+1;
64          end
65      end
66      for n = 3
67          for p = 0:1
68              x_mn = zerobess('J',m,n);
69              x_mn = x_mn(end);
70              freq = (299792458/(2*pi))*sqrt(x_mn^2/R^2+p^2*pi^2/d1^2);
71              freqGHz = freq*1e-9;
72              A(i,1)= m*100+n*10+p;
73              A(i,2)= freqGHz;
74              i=i+1;
75          end
76      end
77  end
78  %Now A is a 32x2 matrix
79
80  %TE
81  for m = 0:3
82      for n = 1:2
83          for p = 1:2
84              xp_mn = zerobess('DJ',m,n); % Calulate the first n zeros of the ...
                    first derivative of the Bessel function of the first kind: ...
                    J_m'(x) = 0
85              xp_mn = xp_mn(end);
86              freq = (299792458/(2*pi))*sqrt(xp_mn^2/R^2+p^2*pi^2/d1^2);
87              freqGHz = freq*1e-9;
88              A(i,1)= m*100+n*10+p;
89              A(i,2)= freqGHz;
90              i=i+1;
91          end
92      end
93      for n = 3
94          for p = 1
95              xp_mn = zerobess('DJ',m,n);
96              xp_mn = xp_mn(end);
97              freq = (299792458/(2*pi))*sqrt(xp_mn^2/R^2+p^2*pi^2/d1^2);
98              freqGHz = freq*1e-9;
99              A(i,1)= m*100+n*10+p;
100             A(i,2)= freqGHz;
101             i=i+1;
102         end
103     end
104 end
105 %Now A is a 52x2 matrix
106
107 %%Calculate the frequencies for the second cavity (R,d2)
108 B=[];
109 j=1;
110
111 %TM
112 for m = 0:3
113     for n = 1:2
114         for p = 0:2
115             x_mn = zerobess('J',m,n);
116             x_mn = x_mn(end);
117             freq = (299792458/(2*pi))*sqrt(x_mn^2/R^2+p^2*pi^2/d2^2);
118             freqGHz = freq*1e-9;
119             B(j,1)= m*100+n*10+p;
120             B(j,2)= freqGHz;
121             j=j+1;
122         end
123     end
124     for n = 3
125         for p = 0:1
```

```
126             x_mn = zerobess('J',m,n);
127             x_mn = x_mn(end);
128             freq = (299792458/(2*pi))*sqrt(x_mn^2/R^2+p^2*pi^2/d2^2);
129             freqGHz = freq*1e-9;
130             B(j,1)= m*100+n*10+p;
131             B(j,2)= freqGHz;
132             j=j+1;
133         end
134     end
135 end
136
137 %TE
138 for m = 0:3
139     for n = 1:2
140         for p = 1:2
141             xp_mn = zerobess('DJ',m,n); % Calulate the first n zeros of the ...
                    first derivative of the Bessel function of the first kind: ...
                    J_m'(x) = 0
142             xp_mn = xp_mn(end);
143             freq = (299792458/(2*pi))*sqrt(xp_mn^2/R^2+p^2*pi^2/d2^2);
144             freqGHz = freq*1e-9;
145             B(j,1)= m*100+n*10+p;
146             B(j,2)= freqGHz;
147             j=j+1;
148         end
149     end
150     for n = 3
151         for p = 1
152             xp_mn = zerobess('DJ',m,n);
153             xp_mn = xp_mn(end);
154             freq = (299792458/(2*pi))*sqrt(xp_mn^2/R^2+p^2*pi^2/d2^2);
155             freqGHz = freq*1e-9;
156             B(j,1)= m*100+n*10+p;
157             B(j,2)= freqGHz;
158             j=j+1;
159         end
160     end
161 end
162
163 %%Plot the spectrum and modes in one graph
164 figure(1);
165 hold on
166 box on
167 plot(1e-6*Vector_1, data1CH0(indexToPlot,:),'-k')
168 plot(1e-6*Vector_3, data3CH0(indexToPlot,:),'--r')
169 for i=33:52
170     if A(i,2)≥ 2 && A(i,2)≤ 8
171         line([A(i,2) A(i,2)],[-2000 -400]) %These values have to be adjusted ...
                according to the measured response.
172         text(A(i,2),-400, ...
                num2str(A(i,1)),'VerticalAlignment','bottom','HorizontalAlignment','center') ...
                %-400 can be changed.
173     end
174 end
175 xlabel('Frequency (GHz)')
176 ylabel('Response (mV)')
177 title('TE modes 135x40.1')
178 legend('Vacuum', 'Argon plasma', 'Location','NorthWest')
179 hold off
180
181 figure(2);
182 hold on
183 box on
184 plot(1e-6*Vector_1, data1CH0(indexToPlot,:),'-k')
185 plot(1e-6*Vector_3, data3CH0(indexToPlot,:),'--r')
186 for i=1:32
187     if A(i,2)≥ 2 && A(i,2)≤ 8
188         line([A(i,2) A(i,2)],[-2000 -400])
189         text(A(i,2),-400, ...
                num2str(A(i,1)),'VerticalAlignment','bottom','HorizontalAlignment','center')
```

```
    end
end
xlabel('Frequency (GHz)')
ylabel('Response (mV)')
title('TM modes 135x40.1')
legend('Vacuum', 'Argon plasma', 'Location','NorthWest')
hold off

figure(3);
hold on
box on
plot(1e-6*Vector_2, data2CH0(indexToPlot,:),'-k')
plot(1e-6*Vector_4, data4CH0(indexToPlot,:),'--r')
for j=33:52
    if B(j,2)≥ 2 && B(j,2)≤ 8
        line([B(j,2) B(j,2)],[-2000 -1300])
        text(B(j,2),-1300, ...
            num2str(B(j,1)),'VerticalAlignment','bottom','HorizontalAlignment','center')
    end
end
xlabel('Frequency (GHz)')
ylabel('Response (mV)')
title('TE modes 135x30.1')
legend('Vacuum', 'Argon plasma', 'Location','NorthWest')
hold off

figure(4);
hold on
box on
plot(1e-6*Vector_2, data2CH0(indexToPlot,:),'-k')
plot(1e-6*Vector_4, data4CH0(indexToPlot,:),'--r')
for j=1:32
    if B(j,2)≥ 2 && B(j,2)≤ 8
        line([B(j,2) B(j,2)],[-2000 -1300])
        text(B(j,2),-1300, ...
            num2str(B(j,1)),'VerticalAlignment','bottom','HorizontalAlignment','center')
    end
end
xlabel('Frequency (GHz)')
ylabel('Response (mV)')
title('TM modes 135x30.1')
legend('Vacuum', 'Argon plasma', 'Location','NorthWest')
hold off
```

A.2 Zerobess function

```
function x = zerobess(funstr,nu,m)
%ZEROBESS Zeros of Bessel functions/derivatives of 1st and 2nd kind.
%   X = ZEROBESS('J',NU,M) finds M positive zeros of the Bessel function
%   of the 1st kind, J_nu(X). The order NU is a real number in the range
%   0 to 1e7. Default is NU = 0 and M = 5.
%
%   ZEROBESS('Y',NU,M) - Zeros of the Bessel function the 2nd kind, Y_nu.
%   ZEROBESS('DJ',NU,M) - Zeros of the derivative of J_nu.
%   ZEROBESS('DY',NU,M) - Zeros of the derivative of Y_nu.
%
%   Examples
%       zerobess('J')
%       zerobess('Y',pi,10)
%       zerobess('DJ',1e-6)
%       zerobess('DY',1e6)
%       tic, x = zerobess('J',25,1e4); toc
%
%   See also BESSELJ, BESSELY

%   2010-02-10  Original ZEROBESS.
%   2010-11-09  Zeros of derivatives added.

%   Author: jonas.lundgren@saabgroup.com, 2010.

if nargin < 1 || isempty(funstr), funstr = 'J'; end
if nargin < 2 || isempty(nu), nu = 0; end
if nargin < 3 || isempty(m), m = 5; end

% Check FUNSTR
if ~ischar(funstr)
    message = 'Function name FUNSTR must be a string.';
    error('ZEROBESS:NoString',message)
else
    funstr = upper(funstr);
end

% Check NU
if numel(nu) ~= 1 || ~isfinite(nu) || ~isreal(nu) || nu < 0 || nu > 1e7
    message = 'Order NU must be a real number between 0 and 1e7.';
    error('ZEROBESS:InvalidNU',message)
end

% Check M
if numel(m) ~= 1 || ~isfinite(m) || ~isreal(m) || m < 1 || fix(m) < m
    message = 'M must be a positive integer.';
    error('ZEROBESS:InvalidM',message)
end

% Set function handle and coefficients
switch funstr
    case 'J'
        fun = @besselj;
        deriv = 0;
        c0 = [  0.1701 -0.6563  1.0355  1.8558
                0.1608 -1.0189  3.1348  3.2447
               -0.2005 -1.2542  5.7249  4.3817 ];
    case 'Y'
        fun = @bessely;
        deriv = 0;
        c0 = [ -0.0474 -0.2300  0.2409  0.9316
                0.2329 -0.8871  2.0165  2.5963
                0.0013 -1.1220  4.3729  3.8342 ];
    case 'DJ'
        fun = @besselj;
        deriv = 1;
        c0 = [ -0.3601 -0.0233  0.0247  0.8087
```

```
                0.2232  -0.9275   1.9605   2.5781
                0.0543  -1.2050   4.3450   3.8258 ];
    case 'DY'
        fun = @bessely;
        deriv = 1;
        c0 = [  0.0116  -0.5561   0.9224   1.8212
                0.1766  -1.0713   3.0923   3.2329
               -0.1650  -1.3116   5.6956   4.3752 ];
    otherwise
        message = '''%s'' is not a valid bessel function.';
        error('ZEROBESS:InvalidName',message,funstr)
end

% Initiate zeros
x = zeros(m,1);

% Initial guess for the first three zeros
x0 = nu + c0*(nu+1).^[-1 -2/3 -1/3 1/3]';

% Exceptional case
n = 0;
if strcmp(funstr,'DJ') && nu < 0.75
    % Correction of initial guess
    x0(1) = sqrt(2*nu)*(((599/9216*nu - 43/384)*nu + 3/8)*nu + 1);
    if nu < 0.0002
        % Skip Newton-Raphson and use asymptotic value
        x(1) = x0(1);
        n = 1;
    end
end

% Newton-Raphson iterations
x(n+1:3) = newton(fun,deriv,nu,x0(n+1:3));

n = 3;  % Number of zeros computed
j = 2;  % Number of zeros to compute next
errtol = 0.005; % Relative error tolerance for initial guess

% Remaining zeros
while n < m

    % Upper bound for j
    j = min(j,m-n);

    % Predict the spacing dx between zeros
    r = diff(x(n-2:n)) - pi;
    if r(1)*r(2) > 0 && r(1)/r(2) > 1
        p = log(r(1)/r(2))/log(1-1/(n-1));
        dx = pi + r(2)*exp(p*log(1+(1:j)/(n-1)))';
    else
        dx = repmat(pi,j,1);
    end

    % Initial guess for zeros
    x0 = x(n) + cumsum(dx);

    % Newton-Raphson iterations
    x(n+1:n+j) = newton(fun,deriv,nu,x0);
    n = n + j;

    % Check zeros
    if ¬chkzeros(nu,x(n-j-1:n),deriv)
        message = 'Bad zeros encountered. NU and/or M may be too large.';
        error('ZEROBESS:BadZeros',message)
    end

    % Relative error
    err = (x(n-j+1:n) - x0)./diff(x(n-j:n));

    % Number of zeros to compute next
```

```
137     if max(abs(err)) < errtol
138         j = 2*j;
139     else
140         j = 2*find(abs(err) ≥ errtol,1);
141     end
142 
143 end
144 
145 % Return
146 x = x(1:m);
147 
148 
149 %---------------------------------------------------------------------------
150 function x = newton(fun,deriv,nu,x0)
151 % Newton-Raphson for Bessel function FUN or FUN' with initial guess X0
152 x = x0;
153 c = 8;
154 for t = 1:10
155     % Newton-Raphson step
156     f = fun(nu,x);
157     g = nu*f./x;
158     df = fun(nu-1,x) - g;
159     if deriv == 0
160         h = -f./df;
161     else
162         ddf = (nu*g - df)./x - f;
163         h = -df./ddf;
164     end
165     x = x + h;
166     % Convergence criteria
167     if all(abs(h) < c*eps(x))
168         break
169     end
170     % Relax convergence criteria
171     if t ≥ 7
172         c = 2*c;
173     end
174 end
175 % Check convergence
176 if t == 10
177     warning('ZEROBESS:Newton','No convergence for Newton-Raphson.')
178 end
179 % fprintf('%2d%8d\n',t,numel(x))
180 
181 
182 %---------------------------------------------------------------------------
183 function s = chkzeros(nu,x,deriv)
184 % Check sequence of Bessel function zeros
185 dx = diff(x);
186 % The spacing dx should decrease except for nu < 0.5
187 ddx = diff(dx);
188 if nu < 0.5 && deriv == 0
189     ddx = -ddx;
190 end
191 % Criteria for acceptable zeros
192 s = isreal(x) && x(1) > 0 && all(dx > 3) && all(ddx < 16*eps(x(2:end-1)));
```